INTERNATIONAL JOURNAL FOR NUMERICAL METHODS IN FLUIDS
Int. J. Numer. Meth. Fluids 2002; **38**:625–645 (DOI: 10.1002/fld.232)

Improved linear interpolation practice for finite-volume schemes on complex grids

T. Lehnhäuser and M. Schäfer*,†

Department of Numerical Methods in Mechanical Engineering, Darmstadt University of Technology, Petersenstr. 30, D-64287 Darmstadt, Germany

SUMMARY

Methods for the computation of flow problems based on finite-volume discretizations and pressure-correction methods frequently require the interpolation of control volume face values from nodal values. The simple, often employed central differencing scheme (CDS) leads to a significant loss in accuracy when the numerical grid is non-regular as it is usual when modelling complex geometries. An alternative technique based on a multi-dimensional Taylor series expansion (TSE) is proposed, which preserves the CDS-like sparsity pattern of the discrete system. While the TSE scheme computationally is only slightly more expensive than the CDS approach, it results in a significantly higher accuracy, where the difference increases with the grid irregularity. The method is investigated and compared to the CDS approach for some representative test cases. Copyright © 2002 John Wiley & Sons, Ltd.

KEY WORDS: finite volume; linear interpolation; complex geometries

1. INTRODUCTION

A very popular class of methods for the numerical solution of flow problems in complex geometries consists of the use of a finite-volume discretization on colocated boundary-fitted grids together with a pressure-correction scheme for the solution of the discrete system. In course of such an approach values of unknowns have to be evaluated repeatedly at the faces of the control volumes (CV) from the values of the nodal points at the CV centres. For this a proper interpolation scheme has to be applied in order to achieve a desired numerical accuracy of the overall discretization scheme.

A standard choice for this interpolation, which is implemented in many commercial and academic CFD packages, is the linear central differencing scheme (CDS) involving the values of two adjacent points to calculate the cell face values (see e.g. Ferziger and Perić [1]). In the one-dimensional case the asymptotic accuracy of this scheme is of second order. In

*Correspondence to: M. Schäfer, Department of Numerical Methods in Mechanical Engineering, Technische Universitat Darmstadt, Petersenstr. 30, 64287 Darmstadt, Germany.
†E-mail: thomas@fnb.tu-darmstadt.de

Contract/grant sponsor: Volkswagen-Stiftung

Received 20 September 2000
Revised 26 June 2000

two or three dimensions the second-order accuracy is only preserved, if the three points involved in the interpolation are connected by a straight line, i.e. if the configuration is quasi one-dimensional. In case of complex grids, which are required for modelling complex geometries, this is usually not fulfilled. The accuracy of the scheme deteriorates in areas, where the grid possesses such irregularities.

Perić [2] investigated this effect for the computation of the convective fluxes for an inviscid stagnation flow. He found unphysical kinks in the pressure distribution when using the linear CDS interpolation together with a distorted grid and proposed grid refinement or grid smoothing to reduce the error. However, since in complex geometries often it is not possible to have a 'nice' grid all over the flow domain, it is much more desirable that the finite-volume solver somehow compensates for the shortcomings of the grid.

Recently, Moulinec and Wesseling [3] investigated several interpolation methods to improve the approximation of derivatives at the cell faces on distorted grids in a finite-element context. For a bilinear interpolation scheme they found significantly improved accuracy and convergence behaviour compared to linear schemes. Barth and Jespersen [4] and Weiss *et al.* [5] propose different interpolations based on Taylor series expansions.

In the present study an interpolation scheme based on a multi-dimensional Taylor series expansion is proposed and investigated. It is designed, on the one hand, to preserve second-order accuracy also on strongly distorted grids without any restriction and, on the other hand, simultaneously, requiring minimum additional effort compared to the CDS approach. The scheme is tested for several representative test cases with varying grid quality and its numerical accuracy is compared to that obtained with the standard CDS.

2. GOVERNING EQUATIONS AND DISCRETIZATION

With no loss of generality we can restrict ourselves to the two-dimensional case, since a generalization of all considered aspects to three dimensions is straightforward. We consider a laminar steady flow of an incompressible Newtonian fluid in an arbitrary domain described by the well-known Navier–Stokes equations:

$$\frac{\partial v_i}{\partial x_i} = 0 \tag{1}$$

$$u_j \frac{\partial u_i}{\partial x_j} = \frac{\partial}{\partial x_j}\left[\nu\left(\frac{\partial u_i}{\partial x_j} + \frac{\partial u_j}{\partial x_i}\right)\right] - \frac{1}{\rho}\frac{\partial p}{\partial x_i} \tag{2}$$

where u_i are the velocity vector components with respect to the Cartesian coordinates x_i, p is the pressure, ν is the kinematic viscosity and ρ is the density (for simplicity, ν and ρ are assumed to be constant).

In order to discretize the conservation Equations (1) and (2) a finite-volume method for general non-orthogonal grids is employed, which is described in detail in Perić [2], Demirdžić and Perić [6], Durst and Schäfer [7]. Here we recall some basics which will be necessary for the following considerations.

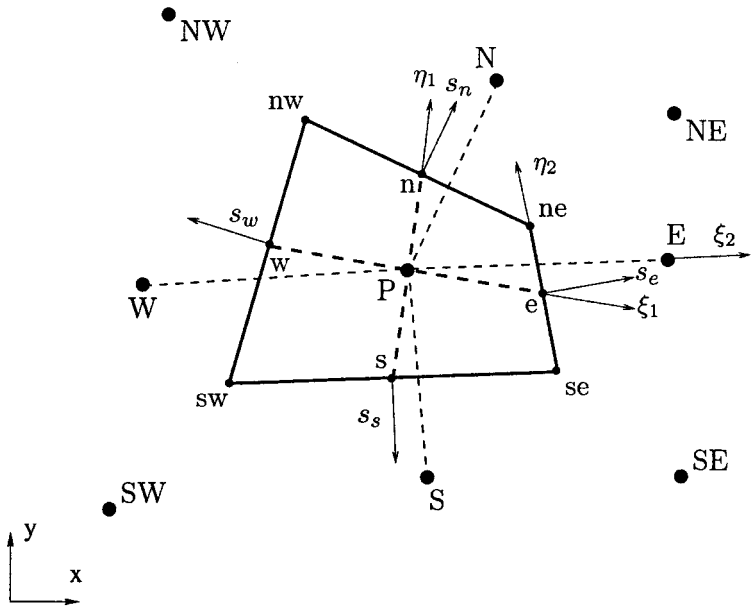

Figure 1. Arbitrary quadrilateral control volume (neighbouring points are labelled according to the compass notation).

Integrating Equations (1) and (2) over an arbitrary quadrilateral control volume (see Figure 1) and applying the Gaussian theorem gives:

$$\sum_c \underbrace{\int_{S_c} u_i n_i \, \mathrm{d}S_c}_{\dot{m}_c} = 0 \tag{3}$$

$$\sum_c \underbrace{\int_{S_c} u_j u_i n_j \, \mathrm{d}S_c}_{F_c^C} = \sum_c \underbrace{\int_{S_c} \nu \left(\frac{\partial u_i}{\partial x_j} + \frac{\partial u_j}{\partial x_i} \right) n_j \, \mathrm{d}S_c}_{F_c^D} - \underbrace{\int_V \frac{1}{\rho} \frac{\partial p}{\partial x_i} \, \mathrm{d}V}_{S^p} \tag{4}$$

where the summation is performed over the four faces of the control volume ($c = e, w, n, s$). The volume integral over the pressure term S^p is approximated by the two-dimensional mid-point rule yielding

$$S^p \approx \frac{1}{\rho} \left(\frac{\partial p}{\partial x_i} \right)_P \delta V \tag{5}$$

where δV is the volume of the corresponding CV. The mass fluxes $\dot{m}_c$, the convective fluxes F_c^C and the diffusive fluxes F_c^D are approximated for each face separately by the

one-dimensional midpoint rule, which, e.g. for the eastern face, yields

$$\dot{m}_e \approx \overline{(u_i)}_e n_i \delta S_e \tag{6}$$

$$F_e^C \approx \dot{m}_e \overline{(u_i)}_e \tag{7}$$

$$F_e^D \approx \nu \left(\left(\frac{\partial u_i}{\partial x_j} \right)_e + \left(\frac{\partial u_j}{\partial x_i} \right)_e \right) n_j \delta S_e \tag{8}$$

where δS_e denotes the length of the eastern face. Here and in the following, the overbar denotes an appropriate interpolation of the cell face value by the nodal values. The method used for this interpolation is the major concern of the present paper and will be discussed in detail in the next section.

For convenience in the following we use the notations $u = u_1$, $v = u_2$ and $x = x_1$, $y = x_2$ and examine the discretization of the u-momentum equation noting that corresponding techniques can be applied in a similar way to the v-momentum equation.

To evaluate the pressure term (Equation (5)) the derivative can be expressed in terms of grid related coordinates ξ_1 and η_1 at point P (see Figure 1). Applying the chain rule one gets

$$\left(\frac{\partial p}{\partial x} \right)_P = \left(\frac{\partial \xi_1}{\partial x} \frac{\partial p}{\partial \xi_1} + \frac{\partial \eta_1}{\partial x} \frac{\partial p}{\partial \eta_1} \right)_P = \frac{1}{J_1} \left(\frac{\partial y}{\partial \eta_1} \frac{\partial p}{\partial \xi_1} - \frac{\partial y}{\partial \xi_1} \frac{\partial p}{\partial \eta_1} \right)_P \tag{9}$$

where

$$J_1 = \frac{\partial x}{\partial \xi_1} \frac{\partial y}{\partial \eta_1} - \frac{\partial x}{\partial \eta_1} \frac{\partial y}{\partial \xi_1} \tag{10}$$

is the Jacobian of the coordinate transformation $(x, y) \leftrightarrow (\xi_1, \eta_1)$. The derivatives of p at node P in the directions ξ_1 and η_1 and the metric terms can be approximated by central differences involving the values at locations e, w, n and s resulting in the approximation

$$\left(\frac{\partial p}{\partial x} \right)_P \approx \frac{(\overline{(p)}_e - \overline{(p)}_w)(y_n - y_s) - (\overline{(p)}_n - \overline{(p)}_s)(y_e - y_w)}{(x_e - x_w)(y_n - y_s) - (x_n - x_s)(y_e - y_w)} \tag{11}$$

Note that the denominator of the right hand side of Equation (11) is equal to the volume δV of the corresponding CV, such that the resulting approximation of the pressure term S^p reads

$$S^p \approx \frac{1}{\rho} [(\overline{(p)}_e - \overline{(p)}_w)(y_n - y_s) - (\overline{(p)}_n - \overline{(p)}_s)(y_e - y_w)] \tag{12}$$

For the further approximation of the diffusive fluxes F_c^D one can express the derivatives in Equation (8) in terms of the grid related coordinates ξ_2 and η_2 (see Figure 1) yielding, e.g. for the derivative of u in x-direction at the east face, the expression

$$\left(\frac{\partial u}{\partial x} \right)_e = \left(\frac{\partial \xi_2}{\partial x} \frac{\partial u}{\partial \xi_2} + \frac{\partial \eta_2}{\partial x} \frac{\partial u}{\partial \eta_2} \right)_e = \frac{1}{J_2} \left(\frac{\partial y}{\partial \eta_2} \frac{\partial u}{\partial \xi_2} - \frac{\partial y}{\partial \xi_2} \frac{\partial u}{\partial \eta_2} \right)_e \tag{13}$$

where J_2 is the Jacobian of the coordinate transformation $(x, y) \leftrightarrow (\xi_2, \eta_2)$. The derivatives of u at point e can be approximated by central differences involving points E and P for the

ξ_2-direction and points *ne* and *se* for the η_2-direction yielding together with a central difference approximation of the metric quantities:

$$\left(\frac{\partial u}{\partial x}\right)_e \approx \frac{1}{\Gamma}[(u_E - u_P)(y_{ne} - y_{se}) - (u_{ne} - u_{se})(y_E - y_P)] \tag{14}$$

with

$$\Gamma = (y_{ne} - y_{se})(x_E - x_P) - (x_{ne} - x_{se})(y_E - y_P) \tag{15}$$

Evaluating $(\partial u/\partial y)_e$ and $(\partial v/\partial x)_e$ in the same manner the approximation of the diffusive flux through the east CV face becomes:

$$\begin{aligned} F_e^D \approx & -\frac{v}{\Gamma}((u_E - u_P)[2(y_{ne} - y_{se})^2 + (x_{ne} - x_{se})^2] \\ & - (\overline{(u)}_{ne} - \overline{(u)}_{se})[2(y_E - y_P)(y_{ne} - y_{se}) + (x_E - x_P)(x_{ne} - x_{se})] \\ & - [(v_E - v_P)(y_{ne} - y_{se}) - (\overline{(v)}_{ne} - \overline{(v)}_{se})(y_E - y_P)](x_{ne} - x_{se})) \end{aligned} \tag{16}$$

Eventually, one can obtain discrete momentum equations of the form:

$$a_P^u u_P + \sum_C a_C^u u_C = b^u, \quad a_P^v v_P + \sum_C a_C^v v_C = b^v \tag{17}$$

where $C = E, W, N, S$ denotes the midpoint of the neighbouring CV. $a_P^u, a_C^u, a_P^v, a_C^v$ represent the corresponding coefficients and b^u, b^v the source terms of the discrete u- and v-momentum equations, respectively.

To solve the coupled system of discrete equations an iterative pressure-correction technique is employed in which again interpolations to the CV faces are necessary. Thus, we also briefly outline the corresponding parts of a variant of the well-known SIMPLE algorithm of Patankar and Spalding [8] as a typical representative of such a method. An extensive description of the applied procedure can also be found in Ferziger and Perić [1]. In a first step provisional velocity components u^* and v^* are computed by evaluating the discrete momentum Equation (17) with an estimated pressure field p^*. Calculating the mass fluxes $\dot{m}_c^*$ with these velocities the continuity equation is not fulfilled but leaving a mass source b_m for each CV:

$$b_m(u_c^*, v_c^*) = \sum_c \dot{m}_c^*(u_c^*, v_c^*) \tag{18}$$

In a next step corrections u', v' and p' to u^*, v^* and p^*, respectively, are sought such that the corrected values exactly fulfil the discrete continuity equation. Subtracting Equation (18) from Equation (3) yields an equation for the mass flux correction which is a function of the velocity corrections:

$$\sum_c \dot{m}_c'(u_c', v_c') = b_m(u_c^*, v_c^*) \tag{19}$$

In the spirit of the SIMPLE algorithm from the momentum equations the following expressions for the velocity corrections can be derived:

$$u_P' = -\frac{\delta V}{\rho a_P^u}\left(\frac{\partial p'}{\partial x}\right)_P \quad \text{and} \quad v_P' = -\frac{\delta V}{\rho a_P^v}\left(\frac{\partial p'}{\partial y}\right)_P \tag{20}$$

To determine the correction at the CV faces without introducing oscillations due to the colocated CV arrangement the selective interpolation technique of Rhie and Chow [9] is employed, which, e.g. for the u-velocity at the east CV face, reads:

$$u'_e = -\overline{\left(\frac{y_n - y_s}{\rho a_P^u}\right)}_e (p'_E - p'_P) \tag{21}$$

Similar formulae result for the other CV faces and for v'. Substituting these expressions into Equation (19) yields the equation for the pressure correction p'.

The velocities u_c^* and v_c^* at the CV faces for assembling the mass source b_m are computed by rewriting the discretized momentum equations for every computational node, e.g. for the velocity component u:

$$u_P^* = \frac{1}{a_P^u}\left(\sum_C a_C^u u_C^* + S^u - \frac{1}{\rho}\left[(\overline{(p)}_e - \overline{(p)}_w)(y_n - y_s) - (\overline{(p)}_n - \overline{(p)}_s)(y_e - y_w)\right]\right) \tag{22}$$

For computing convenience the right-hand side is transformed by using Equation (22) itself yielding the trivial relation:

$$u_P^* = u_P^* + \frac{1}{\rho a_P^u}(\overline{(p)}_e - \overline{(p)}_w)(y_n - y_s) - \frac{1}{\rho a_P^u}(\overline{(p)}_e - \overline{(p)}_w)(y_n - y_s) \tag{23}$$

Since the velocities are needed on the faces of the CV the right-hand side of Equation (23) has to be interpolated with treating the pressure terms differently. Thus, the pressure weighted interpolation is obtained (for details see also Miller and Schmidt [10]). For instance, for u_e^* the corresponding formula reads:

$$u_e^* = (\overline{u^*})_e + \overline{\left(\frac{(\overline{(p)}_e - \overline{(p)}_w)(y_n - y_s)}{\rho a_P^u}\right)} - \overline{\left(\frac{y_n - y_s}{\rho a_P^u}\right)}_e (p_E - p_P) \tag{24}$$

Finally, we can introduce Equations (21) and (24) into Equation (19) to get an equation for the pressure correction p':

$$a_P^p p'_P + \sum_C a_C^p p'_C = b_m(u^*, v^*) \tag{25}$$

After solving Equation (25) one can use p' to correct the pressure p^* and the velocities u^* and v^* (exploiting Equation (20)). Since now the updated velocity and pressure fields fulfil the continuity equation but not the momentum equations any more the procedure has to be repeated until both the momentum and the continuity restriction are fulfilled within a given tolerance.

3. INTERPOLATION SCHEMES

To complete the discretization, for all values noted with an overbar in the deduced equations of the previous section, i.e. in Equations (6), (7), (12), (16), (21) and (24), an interpolation from values at the nodal points in the CV centres (subscripted with uppercase letters) has to be applied. To retain an overall order of two (all other approximations employed are

second-order accurate) the applied interpolation is desired to be also of second order. For this purpose two principle methods will be considered here: the standard CDS interpolation and an approach based on a multi-dimensional Taylor series expansion. The description of the methods is provided exemplarily for the points *e* and *ne*.

3.1. Central differencing scheme

The frequently used CDS is based on the Taylor series expansion

$$\phi_e = \gamma_P \phi_P + \gamma_E \phi_E + \underbrace{\lambda_x \left(\frac{\partial \phi}{\partial x}\right)_e + \lambda_y \left(\frac{\partial \phi}{\partial y}\right)_e + \mathrm{HOT}}_{\text{truncation error}} \tag{26}$$

by skipping the terms indicated as truncation error. In Equation (26) HOT denotes higher order terms and the interpolation factors γ_P, γ_E and the coefficients λ_x, λ_y are defined by

$$\gamma_P = \frac{\sqrt{(x_E - x_e)^2 + (y_E - y_e)^2}}{\sqrt{(x_E - x_P)^2 + (y_E - y_P)^2}} \tag{27}$$

$$\gamma_E = \frac{\sqrt{(x_P - x_e)^2 + (y_P - y_e)^2}}{\sqrt{(x_E - x_P)^2 + (y_E - y_P)^2}} \cong 1 - \gamma_P \tag{28}$$

$$\lambda_x = (x_P - x_e)\gamma_P + (x_E - x_e)\gamma_E \tag{29}$$

$$\lambda_y = (y_P - y_e)\gamma_P + (y_E - y_e)\gamma_E \tag{30}$$

Formally, the CDS approximation only is of first-order accuracy. Second order is achieved if both λ_x and λ_y vanish, which is equivalent to the geometrical constraints (see Figure 2):

$$\underbrace{\frac{x_P - x_e}{\sqrt{(x_P - x_e)^2 + (y_P - y_e)^2}}}_{-\cos\alpha_1} + \underbrace{\frac{x_E - x_e}{\sqrt{(x_E - x_e)^2 + (y_E - y_e)^2}}}_{\cos\alpha_2} = 0 \tag{31}$$

$$\underbrace{\frac{y_P - y_e}{\sqrt{(x_P - x_e)^2 + (y_P - y_e)^2}}}_{-\sin\alpha_1} + \underbrace{\frac{y_E - y_e}{\sqrt{(x_E - x_e)^2 + (y_E - y_e)^2}}}_{\sin\alpha_2} = 0 \tag{32}$$

Hence, the CDS interpolation is of second order, only if $\alpha_1 = \alpha_2$. For grids covering complex geometries this condition usually cannot be fulfilled throughout the whole problem domain resulting in a loss of accuracy depending on the severeness of the grid distortion. Note that in case of $\alpha_1 = \alpha_2$ the interpolation factor γ_E is equal to $1 - \gamma_P$ as indicated in Equation (28). Otherwise the relation holds only approximately but is still used to keep the interpolation consistent accepting a certain error.

Concerning the interpolation in the corner points of the CV, e.g. point *ne*, there is no reason to expect this point in a specific position relative to the computational nodes *P*, *E*, etc. Thus,

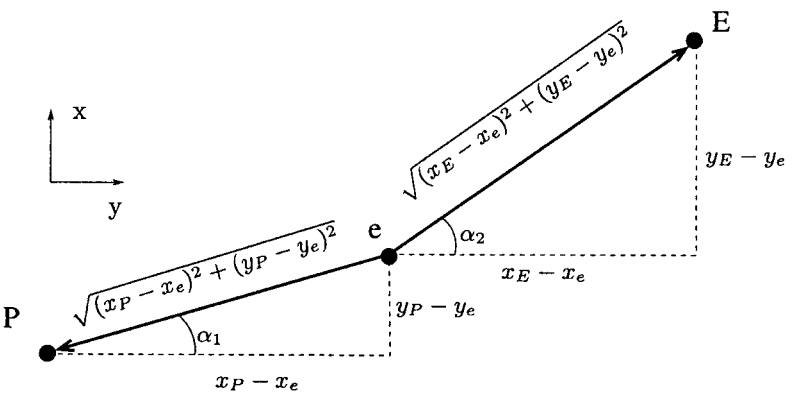

Figure 2. Geometrical interpretation of the accuracy of CDS in two dimensions.

one cannot employ the simple CDS as described above. A simple and often employed way of performing this interpolation is to apply CDS first between E and P and between NE and N. Then, the obtained two values can be interpolated again using CDS with a suitable interpolation factor (e.g. the one corresponding to points P and N). Again, this leads to a deterioration of the accuracy on distorted grids, while on orthogonal grids second order is achieved.

3.2. Interpolation using Taylor series expansions

One straightforward possibility to preserve second-order accuracy as well on distorted grids would be to apply a bilinear interpolation in all cases by taking the exact position of points e and ne into account. However, this approach has two drawbacks. First, it is ambiguous which four nodal points should be taken as the bases for the interpolation, since, for instance, the point e may be located either in the quadrilateral formed by E,P,N,NE or E,P,S,SE (see Figure 3). Second, the bilinear scheme produces relatively large computational molecules leading to an increased number of matrix entries or, if the additional entries are treated explicitly (see e.g. Ferziger and Perić [1]), to an increased number of iterations for solving the corresponding algebraic equation system. Therefore, one can consider alternative methods basing directly on a Taylor series expansions.

3.2.1. Review: Existing methods. A Taylor series expansion about point P for e in two dimensions reads:

$$\phi_a = \phi_P + (x_e - x_P)\left(\frac{\partial \phi}{\partial x}\right)_P + (y_e - y_P)\left(\frac{\partial \phi}{\partial y}\right)_P + \mathrm{HOT} \tag{33}$$

where a denotes a point in the vicinity of P, e.g. e, ne. This approach has been suggested by different authors, e.g. Barth and Jespersen [4], Ferziger and Perić [1] and Weiss *et al.* [5]. They all proceed by evaluating the gradient at point P by the auxiliary expressions:

$$\left[\frac{\partial \phi}{\partial x}\right]_P \approx \frac{1}{\delta\Omega} \oint \phi n^x \, \mathrm{d}s, \qquad \left[\frac{\partial \phi}{\partial y}\right]_P \approx \frac{1}{\delta\Omega} \oint \phi n^y \, \mathrm{d}s \tag{34}$$

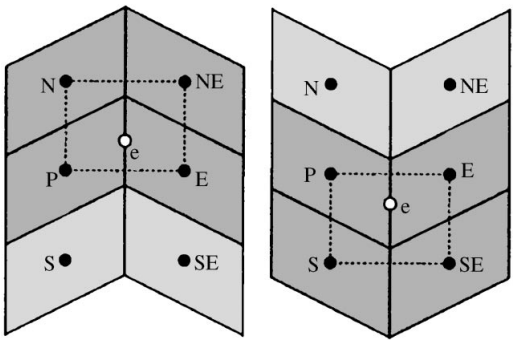

Figure 3. Relative location of CV face values to nodal points.

where $\delta\Omega$ is the area enclosed by the integration path and n^x, n^y are the components of the corresponding surface vector. The approaches of the authors differ in the approximation of the integral. Ferziger and Perić use Equation (33) to interpolate a value of ϕ to an arbitrary point within the CV around P. They assume that ϕ can be represented properly on the surface of the CV and use the approximation:

$$\oint \phi n^x \, \mathrm{d}s \approx \sum_c \phi_c \delta S_c^x \tag{35}$$

Thus, one is again left with the problem to approximate ϕ_c.

Weiss *et al.* [5] use the same integral approximation (Equation (35)) employing Equation (33) as an interpolation formula for ϕ_c. To overcome the problem that ϕ_c is needed to interpolate ϕ_c they use the simple approximation:

$$\phi_c \approx \frac{1}{2}(\phi_C + \phi_P) \tag{36}$$

It is obvious that this approximation leads to a loss in accuracy on distorted grids. Nevertheless, we consider this interpolation for a comparison. It is used in the form:

$$\phi_e = \gamma_P \phi_P + \gamma_E \phi_E + \gamma_W \phi_W + \gamma_N \phi_N + \gamma_S \phi_S \tag{37}$$

We omit the exact definition of the interpolation factors γ_C and just note that the relation between the factors is

$$\gamma_P = 1 - (\gamma_E + \gamma_W + \gamma_N + \gamma_S) \tag{38}$$

Barth and Jespersen [4] propose to integrate for the approximations (Equation (34)) over all nodes whose CV share a common corner point with the CV around P. Hence, in our case the integration path would follow the eight computational points $E, SE, S, SW, W, NW, N, NE$. On the one hand the approximation of the integral can be performed very accurately since no interpolation is needed. On the other hand it is very expensive either to perform this integration whenever an interpolation is needed or to store the eight corresponding interpolation factors. Additionally, the number of matrix entries would be increased. Therefore, we do not consider this method here.

3.2.2. New approach (TSE). Since all above interpolation methods have their drawbacks, it is our objective to design a rule which is cheap to apply and as accurate as possible. The starting point is a Taylor series expansion around point e for an arbitrary point A in the vicinity of e.

$$\phi_A = \phi_e + (x_C - x_e)\left(\frac{\partial\phi}{\partial x}\right)_e + (y_C - y_e)\left(\frac{\partial\phi}{\partial y}\right)_e + \text{HOT} \tag{39}$$

Neglecting the higher order terms, Equation (39) contains three unknowns, namely the value ϕ_e and the two derivatives $(\partial\phi/\partial x)_e$ and $(\partial\phi/\partial y)_e$.

Evaluating Equation (39) for at least three known points, e.g. P, E and N, one can eliminate the two derivatives leading to a formula for ϕ_e, which may be unsolvable due to geometrical constraints. Therefore, a better choice is to solve for the derivatives in a first step. For symmetry reasons we choose the Taylor series expansions for the points P, E, N and S, with which the derivatives can be approximated by

$$\left(\frac{\partial\phi}{\partial x}\right)_e \approx \frac{1}{\Theta}[(\phi_E - \phi_P)(y_N - y_S) - (\phi_N - \phi_S)(y_E - y_P)] \tag{40}$$

$$\left(\frac{\partial\phi}{\partial y}\right)_e \approx \frac{1}{\Theta}[(\phi_N - \phi_S)(x_E - x_P) - (\phi_E - \phi_P)(x_N - x_S)] \tag{41}$$

with

$$\Theta = (x_E - x_P)(y_N - y_S) - (x_N - x_S)(y_E - y_P) \tag{42}$$

Note that Θ describes the area spanned by the vectors pointing from E to P and from N to S. Since these two vectors never coincide on structured grids, Θ always is different from zero. Substituting Equations (40) and (41) into the Taylor series expansion for point P gives:

$$\begin{aligned}\phi_e \approx \phi_P &- \frac{x_P - x_e}{\Theta}[(\phi_E - \phi_P)(y_N - y_S) - (\phi_N - \phi_S)(y_E - y_P)] \\ &- \frac{y_P - y_e}{\Theta}[(\phi_N - \phi_S)(x_E - x_P) - (\phi_E - \phi_P)(x_N - x_S)]\end{aligned} \tag{43}$$

The approximation provided by Equation (43) is second-order accurate, independent of the grid. Similar to the expression for CDS it can be rewritten in the form

$$\phi_e \approx \gamma_P\phi_P + \gamma_E\phi_E + \gamma_N\phi_N + \gamma_S\phi_S \tag{44}$$

with

$$\gamma_P = 1 + \frac{1}{\Theta}[(x_P - x_e)(y_N - y_S) - (y_P - y_e)(x_N - x_S)] \tag{45}$$

$$\gamma_E = \frac{1}{\Theta}[-(x_P - x_e)(y_N - y_S) + (y_P - y_e)(x_N - x_S)] \tag{46}$$

$$\gamma_N = \frac{1}{\Theta}[(x_P - x_e)(y_E - y_P) - (y_P - y_e)(x_E - x_P)] \tag{47}$$

$$\gamma_S = \frac{1}{\Theta}[-(x_P - x_e)(y_E - y_P) + (y_P - y_e)(x_E - x_P)] \tag{48}$$

Observe that $\gamma_E = 1 - \gamma_P$ and $\gamma_S = -\gamma_N$.

For the interpolation of the corner value ϕ_{ne} a formula similar to Equation (44) can be derived, where again the values at the points P, E, N and S serve as the basis for the interpolation. In this case the corresponding interpolation factors read:

$$\gamma_P = 1 + \frac{1}{\Theta}[(x_P - x_{ne})(y_N - y_S) - (y_P - y_{ne})(x_N - x_S)] \tag{49}$$

$$\gamma_E = \frac{1}{\Theta}[-(x_P - x_{ne})(y_N - y_S) + (y_P - y_{ne})(x_N - x_S)] \tag{50}$$

$$\gamma_N = \frac{1}{\Theta}[(x_P - x_{ne})(y_E - y_P) - (y_P - y_{ne})(x_E - x_P)] \tag{51}$$

$$\gamma_S = \frac{1}{\Theta}[-(x_P - x_{ne})(y_E - y_P) + (y_P - y_{ne})(x_E - x_P)] \tag{52}$$

Again the factors follow the correlations $\gamma_E = 1 - \gamma_P$ and $\gamma_S = -\gamma_N$.

4. NUMERICAL RESULTS

To investigate the accuracy of the TSE scheme and compare it to the other schemes indicated in the previous section, two test cases (Sections 4.1 and 4.2), for which analytical solutions are known, as well as a more practical example (Section 4.3) are considered.

To quantify the accuracy of the schemes an error is evaluated by the volume weighted summation of the mean errors at all computational points:

$$E_\phi = \frac{1}{\delta\Gamma} \sum_{\mathrm{CV}} \delta V \frac{\phi_{\mathrm{analytical}} - \phi_{\mathrm{numerical}}}{\phi_{\mathrm{analytical}}} \tag{53}$$

where δV is the volume of the corresponding CV and $\delta\Gamma$ is the volume of the whole problem domain. Orders of convergence are either evaluated from

$$p = \log\left(\frac{E_\phi^{2h}}{E_\phi^h}\right) \Big/ \log 2 \tag{54}$$

or

$$p = \log\left(\frac{\sigma^{4h} - \sigma^{2h}}{\sigma^{2h} - \sigma^h}\right) \Big/ \log 2 \tag{55}$$

where σ denotes a characteristic value and the superscripts $4h, 2h, h$ indicate successively refined grids.

Details of the overall numerical solution procedure employed are given in the paper by Durst and Schäfer [7]. In particular, to enhance the diagonal dominance of the system matrices the convective fluxes are implemented via a deferred correction approach [11], where the second-order parts of the flux approximations are treated explicitly and only the first-order upwind parts are treated implicitly. The employment of a flux-blending coefficient (FBC) offers the opportunity to select either the first-order method (FBC = 0), the second-order method (FBC = 1) or a blending of both (0 < FBC < 1). Note that a value for FBC different from 1 is only considered for the example in Section 4.3.

4.1. Stagnation flow

As a first test case we consider the stagnation flow in a unit square $[0,1]^2$ also discussed by Perić [2]. The analytical solution of the problem is given by

$$u(x) = x, \qquad v(y) = -y, \qquad p(x,y) = p_0 - \frac{\rho}{2}(u^2 + v^2) \tag{56}$$

where p_0 is the pressure at the stagnation point $(x,y) = (0,0)$. Figure 4 illustrates the distribution of the isobars and the streamlines for the flow. The isobars correspond to circles around the stagnation point. We solve the problem numerically on the three types of grids shown in Figure 5 (see also Perić [2]). The first represents a uniform Cartesian grid, which is the obvious choice for a quadratic domain. The second grid includes sharp changes of grid line directions representing a typical class of grid distortions, which can usually be found in any structured grid for complex geometries. The third grid is randomly distorted in both coordinate directions. While the uniform Cartesian grid satisfies the conditions for the CDS interpolation to be of second-order accuracy, the distorted grids do not.

Applying CDS on the systematically distorted grid with different spatial resolutions (with 10×10, 20×20 and 40×40 CVs) one obtains the pressure distributions given in Figure 6. It is obvious that in the vicinity of the kinks in the grid lines the isobars are strongly deteriorated. With grid refinement the error zone becomes narrower, but the general behaviour does not improve. Using the interpolation of Weiss *et al.* [5], as expected from theory, the situation does not improve significantly (see Figure 7). Figure 8 shows the isobars obtained

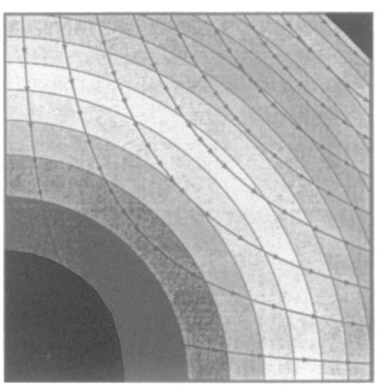

Figure 4. Analytical distribution of isobars and streamlines for the stagnation flow.

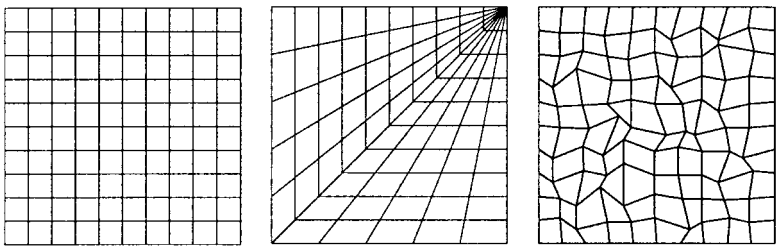

Figure 5. Uniform Cartesian grid (I), systematically distorted grid (II) and randomly distorted grid (III) for the stagnation flow problem.

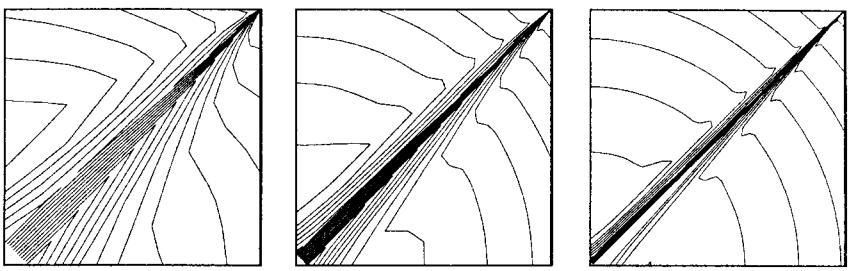

Figure 6. Isobars for the stagnation flow problem on three successively refined grids (distorted grid II) calculated with CDS.

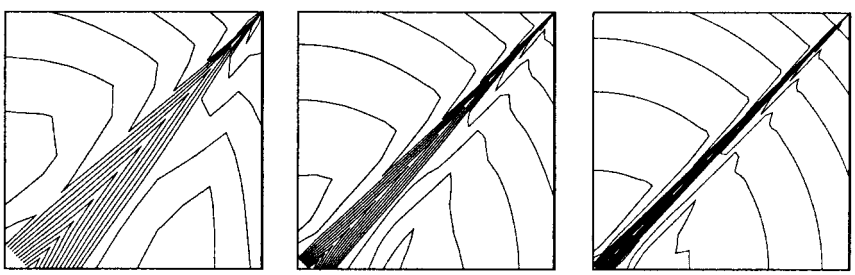

Figure 7. Isobars for the stagnation flow problem on three successively refined grids (distorted grid II) calculated with the interpolation of Weiss *et al.* [5].

on the systematically distorted grids (with the same resolutions as above) when using the TSE interpolation. One can see that the grid geometry does not noticeably affect the accuracy of the solution.

To quantify the accuracy of all three interpolation schemes in Tables I and II the mean relative errors for the velocities and the pressure for the grid setups I and II with different resolutions are summarized. The error on the Cartesian grid using CDS interpolation is already small on the coarsest grid and is reduced remarkably with every refinement. Employment of CDS on the distorted grid leads to severe losses in accuracy. In particular, the error for the

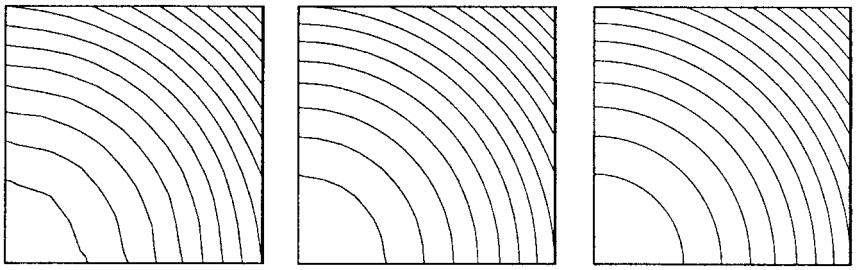

Figure 8. Isobars for the stagnation flow problem on three successively refined grids (distorted grid II) calculated with TSE.

Table I. Relative error of u-velocity E_u obtained with all three interpolations on grids I and II (in per cent) and order of convergence for the stagnation flow problem.

	CDS		Weiss	TSE
			Grid II	Grid II
CV	Grid I	Grid II		
10×10	2.0×10^{-4}	1.9×10^{-2}	9.8×10^{-3}	4.6×10^{-4}
20×20	2.5×10^{-5}	6.3×10^{-3}	3.4×10^{-3}	5.4×10^{-5}
40×40	3.1×10^{-6}	2.1×10^{-3}	1.1×10^{-3}	6.6×10^{-6}
80×80	4.0×10^{-7}	6.5×10^{-4}	3.7×10^{-4}	8.6×10^{-7}
160×160	6.4×10^{-8}	2.1×10^{-4}	1.27×10^{-4}	1.2×10^{-7}
Order	2.6	1.6	1.6	2.8

Table II. Relative error of the pressure E_p obtained with all three interpolations on grids I and II (in per cent) and order of convergence for the stagnation flow problem.

	CDS		Weiss	TSE
			Grid II	Grid II
CV	Grid I	Grid II		
10×10	1.1×10^{-1}	1.1×10^{0}	9.7×10^{-1}	6.5×10^{-2}
20×20	3.0×10^{-2}	9.9×10^{-1}	9.4×10^{-1}	2.9×10^{-2}
40×40	8.1×10^{-3}	9.4×10^{-1}	9.3×10^{-1}	6.2×10^{-3}
80×80	2.2×10^{-3}	9.1×10^{-1}	9.2×10^{-1}	1.7×10^{-3}
160×160	6.0×10^{-4}	9.0×10^{-1}	9.2×10^{-1}	4.9×10^{-4}
Order	1.9	0.0	0.0	1.8

pressure with about 90 per cent is very high. The velocities are not predicted that badly, although the error is several orders of magnitude higher than in the Cartesian case. The same statement holds for the interpolation of Weiss *et al.* [5] although the error is reduced slightly. The situation changes when using the TSE interpolation. The mean errors for both grid types are of the same magnitude. In Tables I and II also the rates of convergence for the velocity

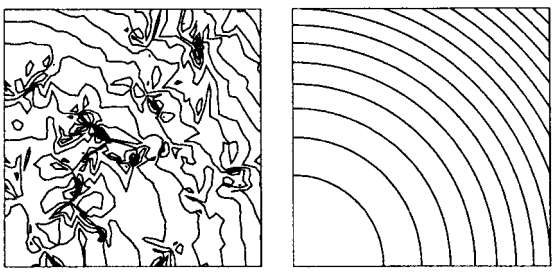

Figure 9. Isobars for the stagnation flow problem on a randomly distorted grid calculated with CDS and TSE.

and pressure is given. Due to the linear distribution of the velocities the leading error term in the momentum equations is of third order. Therefore, we expect an order of three for the velocity although the employed scheme only has an overall order of two. In the Cartesian case we nearly obtain the estimated orders of convergence for velocity and pressure. With the distorted grid one observes a severe loss in the order of convergence, in particular, for the pressure, for which the order is close to zero. As expected, the application of TSE preserves the order on the distorted grid.

Finally, we present the results of the stagnation flow problem on the randomly distorted grid III with CDS and TSE. We omit the interpolation of Weiss *et al.* [5] here and in the following since, as shown before, it does not improve the situation on distorted grids significantly compared to CDS. Figure 9 presents the isobars on a grid with 40×40 CVs. As expected the TSE yields a perfect result while CDS suffer from its deficiencies.

4.2. *Channel flow*

To study the accuracy of the interpolation practices for systematically varying grid quality the laminar Poisseuille flow in a plane channel is considered. The analytical solution reads

$$u(y) = 4 \cdot u_{\max}\left(1 - \frac{y}{h}\right)\frac{y}{h}, \qquad v = 0, \qquad p(x) = p_0 - 8\nu\rho\frac{u_{\max}}{h^2}x \tag{57}$$

where h is the channel height, $u_{\max}$ is the maximum velocity and p_0 is an arbitrary constant. The problem parameters are chosen to yield a Reynolds number of $Re = 200$ based on the channel height.

Again, of course, the natural choice for this problem is a Cartesian grid. To investigate the error due to grid deficiencies three systematically distorted grids are employed (see Figure 10). The grid distortion is characterized by the maximum angle α between the grid lines and the channel walls, for which the values $\alpha = 14°, 26°, 36.5°$ are considered. The Cartesian grid corresponds to $\alpha = 0°$. In Figures 11 and 12 the pressure distribution and the velocity distribution along the channel at $y = 0.7438h$ using both interpolation practices CDS and TSE are presented. The section shown in the direction along the channel corresponds to the first grid line deviation from the horizontal. Using the CDS interpolation the pressure as well as the velocity deviates more and more from the analytical solution with increasing grid distortion. Even small distortions as for $\alpha = 14°$ cause remarkable shortcomings in the numerical solution. Compared to that the pressure distribution on the distorted grids calculated with the

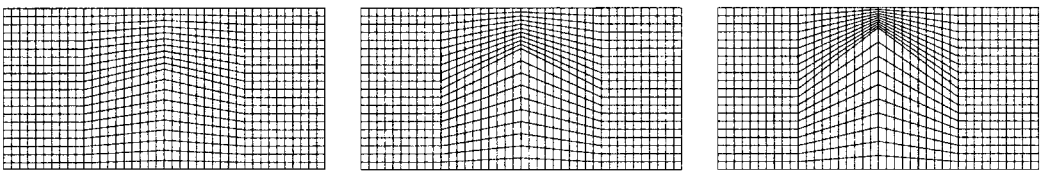

Figure 10. Systematically distorted grids for the channel flow.

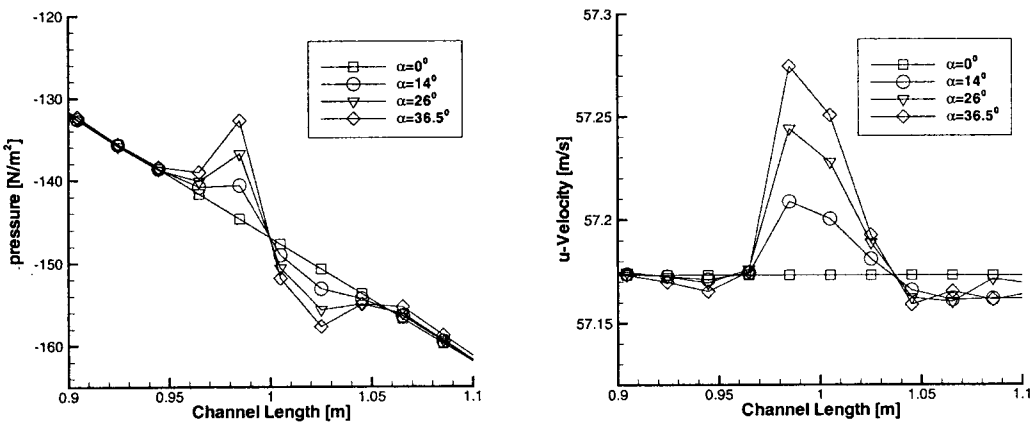

Figure 11. Pressure and velocity distribution for the channel flow computed on a grid with 160×80 CV with CDS.

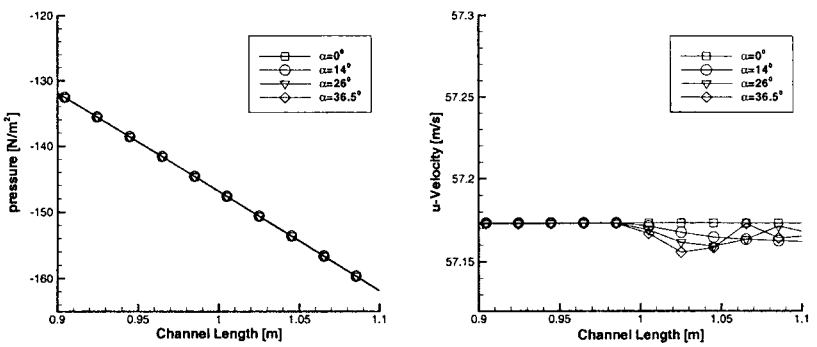

Figure 12. Pressure and velocity distribution for the channel flow computed on a grid with 160×80 CV with TSE.

TSE interpolation fits very well the analytical solution. The velocity distribution still includes observable errors due to the grid distortion but compared to the CDS case they are reduced by a factor of five.

Table III. Relative errors of velocity obtained with both interpolations (in per cent) on systematically distorted grids and orders of convergence for the channel flow problem.

	$\alpha = 14°$		$\alpha = 26°$		$\alpha = 36.5°$	
CV	CDS	TSE	CDS	TSE	CDS	TSE
40×20	7.8×10^{-2}	5.7×10^{-2}	1.5×10^{-1}	7.8×10^{-2}	2.5×10^{-1}	1.1×10^{-1}
80×40	2.1×10^{-2}	1.5×10^{-2}	4.5×10^{-2}	2.0×10^{-2}	7.4×10^{-2}	2.7×10^{-2}
160×80	6.2×10^{-3}	3.7×10^{-3}	1.6×10^{-2}	5.0×10^{-3}	2.7×10^{-2}	6.9×10^{-3}
Order	1.8	2.0	1.5	2.0	1.4	2.0

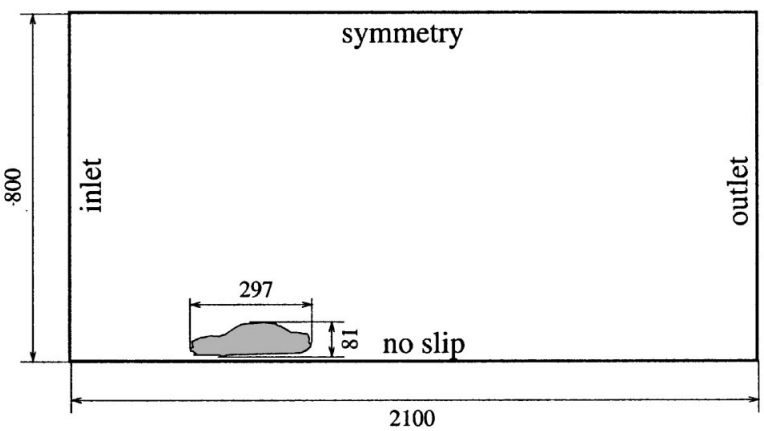

Figure 13. Problem configuration for turbulent flow around a car (lengths indicated in millimeters).

In Table III the global errors for u on the distorted grids using CDS and TSE are summarized for different grid sizes together with the corresponding orders of convergence. Using CDS the order deviates more and more from two with increasing grid distortion, while the employment of TSE ensures that the second order is preserved independent of the grid. Although also with TSE the absolute values of the global error depend on the angle of distortion, in all cases the values are smaller as with CDS, where due to the reduced order of CDS the difference also increases with the grid size. On the grid with $\alpha = 36.5°$ with TSE one gets the same global accuracy with 40×80 CV as with CDS with 160×80 control volumes.

4.3. Flow around a car model

As a more practical test case for the comparison of both interpolation schemes we consider the turbulent flow around a two-dimensional car model, which was already investigated numerically and experimentally by Angelis [12]. The problem geometry is illustrated in Figure 13. At the inlet a measured turbulent mean velocity profile with maximum (averaged) velocity $u_{\max} = 15\,\mathrm{m\,s^{-1}}$ is chosen (see Angelis [12]). The other boundary conditions are: a symmetry condition at the top, a zero gradient condition at the outlet and a no-slip condition at the bottom and around the car. The fluid parameters are that of air giving a Reynolds number

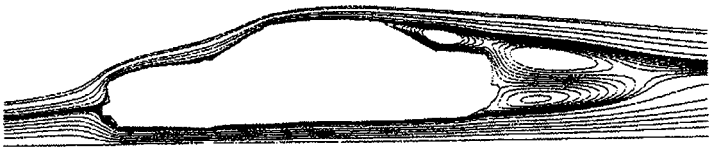

Figure 14. Streamlines for turbulent flow around a car.

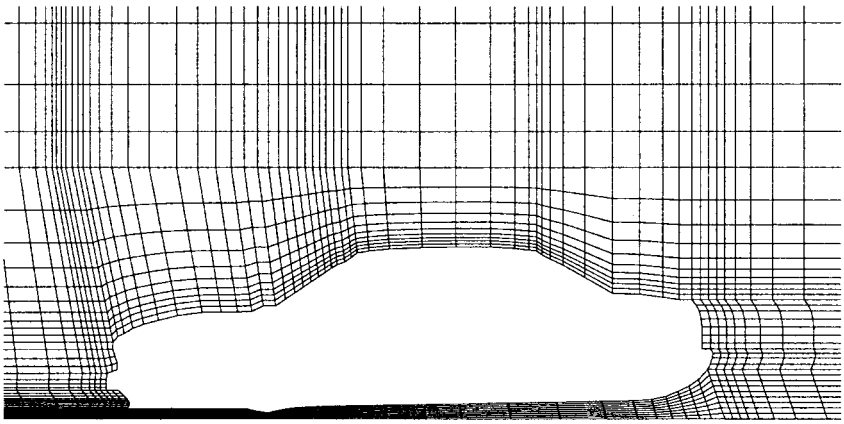

Figure 15. Section of numerical grid for turbulent flow around a car.

of $Re = 338\,000$ based on the length $l = 0.297$ m of the car. The turbulence is accounted for by employing the standard κ–ε model with wall functions (see Launder and Spalding [13]). The inlet values for κ and ε are set according to $\kappa = 0.01u^2$ and $\varepsilon = \kappa^{3/2}/l$. The flow pattern is indicated in Figure 14 showing the streamlines in the area around the car. In the discretization of the transport equations for κ and ε the same techniques as described for the momentum equations are applied, in particular, for the necessary interpolations of values of κ and ε to the CV faces either CDS or TSE is employed. Computations are performed for three successively refined grids with 2774 CVs, 11 096 CVs and 44 384 CVs. In Figure 15 the coarsest numerical grid in the critical region around the car is shown. Note that the grid can be considered to be of rather good quality without much distortion with respect to orthogonality. To see in particular the influence of the considered interpolation practices with respect to the approximation of the convective fluxes in a convection dominated flow two flux-blending coefficients are considered: FBC = 0.0 representing a first-order upwind approximation, i.e. neither TSE nor CDS will be employed in the discretization of the convective fluxes, and FBC = 0.9 resulting in a discretization close to second-order using either TSE or CDS (for higher FBC values convergence problems arise). Figure 16 shows the distributions of the pressure in the rear of the car computed on the finest grid employing TSE and CDS with FBC = 0.9. Although the grid quality is good, locally the pressure is disturbed apparently when employing CDS. Globally, the pressure distributions do not seem to differ too much. However, the drag coefficient, which plays an important role in automotive engineering, can be influenced remarkably even by minor changes in the pressure field. To see this Table IV

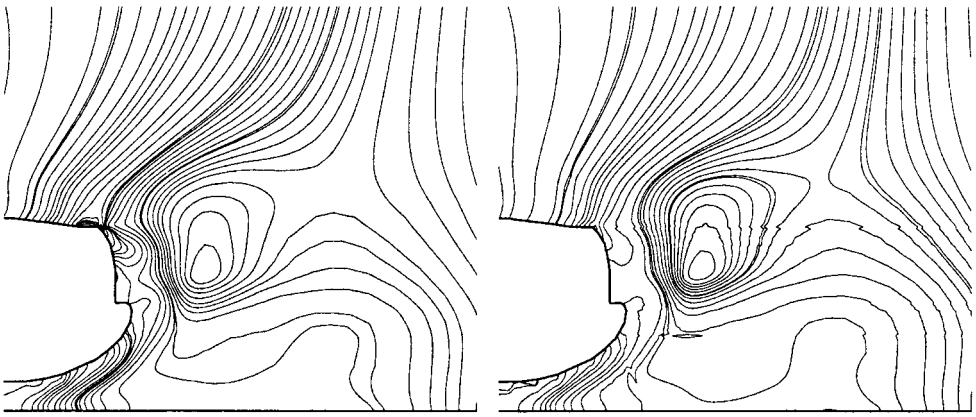

Figure 16. Isobars at the rear of the car obtained with TSE (left) and CDS (right) and 0.9 for the flux-blending coefficient.

Table IV. Drag coefficients, grid-independent solutions (GIS) and orders of convergence with TSE and CDS for two different flux-blending coefficients FBC.

	FBC = 0.0		FBC = 0.9	
CV	TSE	CDS	TSE	CDS
2774	0.5944	0.6212	0.4773	0.4868
11096	0.4920	0.5149	0.4148	0.4280
44384	0.4480	0.4642	0.3972	0.4093
GIS	0.4148	0.4179	0.3903	0.4006
Order	1.2186	1.0681	1.8283	1.6528

presents the values for the drag coefficient computed from the results with both interpolation practices and the two different flux-blending coefficients. Additionally, for every set of parameters the order of convergence and the corresponding extrapolated grid-independent solution is given. The resulting numerical errors for the different grids based on a comparison with the respective grid-independent solution are given in Figure 17. For FBC = 0.0 the order is close to one for both interpolation schemes. While the grid-independent solution is nearly the same, the computed values on the successively refined grid levels differ due to the slightly higher value for the order of convergence when using TSE. Employing FBC = 0.9 with TSE yields an order of convergence of nearly 2, while CDS again suffers from the grid deficiencies. In summary, also for this test case the advantage in accuracy of TSE over CDS is clear.

Finally, to compare the computational costs with TSE and CDS the CPU time for one pressure correction cycle is measured where three linear system relaxations of the momentum equations and the equations for κ and ε and relaxations on the pressure correction equation are performed. The results are summarized in Table V. As the storage cost, the computational cost for one cycle increases only by about 10 per cent on every grid level.

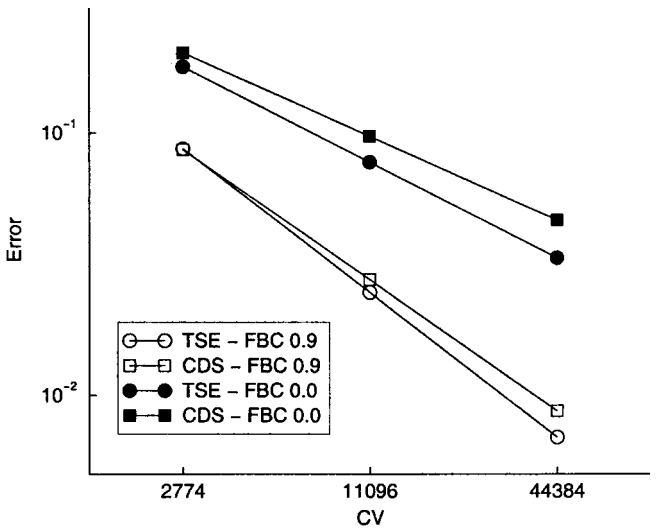

Figure 17. Numerical error in the drag coefficient obtained with TSE and CDS for two different flux-blending coefficients.

Table V. CPU time spend for one pressure correction cycle and until convergence using CDS and TSE in seconds on a SUN ULTRA/1 workstation.

CV	CDS	TSE	Factor
2774	2.0130×10^{-1}	2.1742×10^{-1}	1.08
11096	7.3840×10^{-1}	8.0643×10^{-1}	1.09
44384	2.9191×10^{0}	3.1939×10^{0}	1.09

5. CONCLUSIONS

Since the CDS interpolation is only first-order accurate on distorted grids, the overall accuracy of an otherwise second-order scheme employing this kind of CV face interpolation is reduced significantly when the grid has irregularities. Even more severe than the global loss in the order of convergence is the local error in the vicinity of a grid distortion. In particular, the pressure distribution, which in many engineering applications is a most important quantity (e.g. for lift and drag computations), is very sensitive to this effect.

It was shown that an overall second-order accurate scheme, independent of any grid distortion, can be achieved by using the considered TSE interpolation. Since the scheme preserves the sparsity pattern of the computational molecule, it is only slightly more expensive with respect to computational effort as compared to the CDS scheme. Also the local errors near grid distortions become much smaller with this scheme. Thus, with the TSE interpolation a simple and efficient method for interpolations to CV faces is provided, which ensures second-order accurate numerical solutions also when the numerical grid has deficiencies, which usually are unavoidable when dealing with complex geometries.

ACKNOWLEDGEMENTS

The financial support of the work by the *Volkswagen-Stiftung* is gratefully acknowledged.

REFERENCES

1. Ferziger J, Perić M. *Computational Methods for Fluid Dynamics.* Springer: Berlin, 1996.
2. Perić M. A Finite Volume Method for the Prediction of Three-Dimensional Fluid Flow in Complex Ducts. *PhD thesis*, University of London, 1985.
3. Moulinec C, Wesseling P. Colocated schemes for the incompressible Navier–Stokes equations on non-smooth grids for two-dimensional problems. *International Journal for Numerical Methods in Fluids* 2000; **32**:349–364.
4. Barth TJ, Jespersen DC. The design and application of upwind schemes on unstructured meshes. AIAA Paper 89-0366, Jan 1989.
5. Weiss JM, Maruszewski JP, Smith WA. Implicit solution of preconditioned Navier–Stokes equations using algebraic multigrid. *AIAA Journal* 1999; **37**(1):29–36.
6. Demirdžić I, Perić M. Finite volume method for prediction of fluid flow in arbitrary shaped domains with moving boundaries. *International Journal for Numerical Methods in Fluids* 1990; **10**:771–790.
7. Durst F, Schäfer M. A parallel blockstructured multigrid method for the prediction of incompressible flow. *International Journal for Numerical Methods in Fluids* 1996; **22**:549–565.
8. Patankar SV, Spalding DB. A calculation procedure for heat, mass and momentum transfer in three dimensional parabolic flows. *International Journal for Heat and Mass Transfer* 1972; **15**:1787–1806.
9. Rhie CM, Chow WL. Numerical study of the turbulent flow past an airfoil with trailing edge separation. *AIAA Journal* 1983; **21**:1525–1532.
10. Miller IF, Schmidt FW. Use of a pressure-weighted interpolation method for the solution of the incompressible Navier–Stokes equations on a nonstaggered grid system. *Numerical Heat Transfer* 1983; **14**:213–233.
11. Khosla PK, Rubin SG. A diagonally dominant second-order accurate implicit scheme. *Computer Fluids* 1974; **2**:207–209.
12. Angelis W. Komplementäre Methodik in der Aerodynamik bodennaher Fahrzeuge. *PhD thesis*, Universität Erlangen-Nuremberg, 1996.
13. Launder BE, Spalding DB. The numerical computation of turbulent flows. *Computational Methods in Applied Mechanical Engineering* 1974; **3**:269–289.

